

# Laplacian Convolutional Representation for Traffic Time Series Imputation

Xinyu Chen, Zhanhong Cheng, Nicolas Saunier, Lijun Sun, *Senior Member, IEEE*

**Abstract**—Spatiotemporal traffic data imputation is of great significance in intelligent transportation systems and data-driven decision-making processes. To make an accurate reconstruction from partially observed traffic data, we assert the importance of characterizing both global and local trends in traffic time series. In the literature, substantial prior works have demonstrated the effectiveness of utilizing low-rankness property of traffic data by matrix/tensor completion models. In this study, we first introduce a Laplacian kernel to temporal regularization for characterizing local trends in traffic time series, which can be formulated in the form of circular convolution. Then, we develop a low-rank Laplacian convolutional representation (LCR) model by putting the nuclear norm of a circulant matrix and the Laplacian temporal regularization together, which is proved to meet a unified framework that takes a fast Fourier transform (FFT) solution in a relatively low time complexity. Through extensive experiments on some traffic datasets, we demonstrate the superiority of LCR for imputing traffic time series of various time series behaviors (e.g., data noises and strong/weak periodicity). The proposed LCR model is an efficient and effective solution to large-scale traffic data imputation over the existing baseline models. Despite the LCR's application to time series data, the key modeling idea lies in bridging the low-rank models and the Laplacian regularization through FFT, which is also applicable to image inpainting.

**Index Terms**—Spatiotemporal traffic data, time series imputation, low-rank models, Laplacian regularization, circular convolution, discrete Fourier transform

## I. INTRODUCTION

**M**ISSING data imputation is a fundamental component to a wide range of applications in modern intelligent transportation systems (ITS), such as route planning, travel time estimation, and traffic flow forecasting. As a common sense, traffic data can be collected by fixed traffic sensors (e.g., loop detectors, video cameras, and radars) on a continuous basis, resulting in a sequence of time series for measuring the dynamics of traffic flow. Since real-world ITS often suffers from various operational issues, such as sensor failure and network communication problems, these lead to data corruption and missing values. Making accurate recovery on traffic time series data is important for supporting ITS applications, and still demands appropriate imputation approaches.

For traffic time series, the basic modeling idea of missing data imputation is to exploit the spatial and temporal correlations/dependencies from partial observations. Typically, traffic flow data always show strong global and local trends with long-term and short-term patterns [1]. The global trends refer to certain periodic, seasonal, and cyclical patterns, which can be well characterized by low-rank models. Unfortunately, conventional low-rank models fail to characterize the sequential dynamics of time series because the reconstruction of low-rank models (e.g., low-rank matrix completion (LRMC) [2], [3]) is invariant to the permutation of rows and columns. Therefore, recent studies presented low-rank time series completion models based on certain algebraic structures, including the Hankel matrices/tensors [4], circulant/anti-circulant matrices/tensors [5], [6], and convolution matrices [6], [7]. The sequential dependencies are implicitly captured by delay embedding when characterizing the low-rankness property with these algebraic structures. However, low-rank Hankel/convolution models are always limited to small-/middle-scale problems due to the large size of delay-embedded matrices/tensors. Although circulant matrix nuclear norm minimization (CircNNM) can be efficiently solved via the use of the fast Fourier transform (FFT), compared with Hankel/convolution matrices, circulant matrices have the restricted form and fail to characterize the local trends of time series [6].

Regarding the low-rank framework, the default structure of most low-rank models does not ensure local smoothness/correlation properties. Thus, it requires us to model both global patterns and local trends in a unified low-rank framework. In the literature, there are several ways to characterize the local spatial and temporal dependencies in data-driven machine learning models. For example, on the spatial dimension, Laplacian regularization has become a standard technique to impose local consistency on a network (e.g., [8], [9]). On the temporal dimension, the local smoothness property is often characterized using temporal regularization and time series autoregression explicitly (see e.g., [10], [11], [12]).

Considering the importance of temporal regularization techniques in regulating the behavior of global low-rank models, we are inspired to develop a tailored regularizer for CircNNM to improve its capability of local trends modeling while maintaining the algorithm efficiency through FFT. Therefore, using the fact that the Laplacian matrix of a circulant graph is a circulant matrix, we first introduce a novel Laplacian-matrix-based temporal regularization to the CircNNM problem. Next, we develop an efficient algorithm to solve the proposed Laplacian convolutional representation (LCR) using the alter-

X. Chen and N. Saunier are with the Civil, Geological and Mining Engineering Department, Polytechnique Montreal, Montreal, QC H3T 1J4, Canada. E-mail: chenxy346@gmail.com (X. Chen), nicolas.saunier@polymtl.ca (N. Saunier).

Z. Cheng and L. Sun are with the Department of Civil Engineering, McGill University, Montreal, QC H3A 0C3, Canada. E-mail: zhanhong.cheng@mail.mcgill.ca (Z. Cheng), lijun.sun@mcgill.ca (L. Sun).

(Corresponding author: Nicolas Saunier)

nating direction method of multipliers (ADMM) and FFT. The proposed imputation method is evaluated on several real-world traffic flow datasets. The experimental results demonstrate that the proposed method can achieve better performance than the state-of-the-art baseline methods in terms of both accuracy and efficiency. The contribution of this work is three-fold:

- We introduce a circular Laplacian kernel and use it to define a temporal regularization term for characterizing the local trends in traffic time series. Following that definition, the Laplacian temporal regularization can be formulated as a circular convolution operation.
- We propose a low-rank completion model—LCR—by modeling global trends as the nuclear norm of a circulant matrix and modeling local trends by a Laplacian temporal regularization. According to the properties of the circulant matrix and circular convolution, we present a fast implementation of LCR through FFT.
- We demonstrate the imputation performance of LCR on some real-world traffic flow datasets and verify the importance of Laplacian temporal regularization in LCR. The model is well-suited to sparse traffic flow time series that are characterized by both seasonality and non-seasonality. In addition, due to the fast implementation via FFT with relatively low complexity, the proposed model is scalable to large and high-dimensional imputation problems.

The remainder of this paper is structured as follows. Section II introduces the related work. Section III reviews the basic definitions of circulant matrix and convolution operator in machine learning and signal processing. In Section IV, we present a novel temporal regularization and integrate it into the circulant-matrix-based low-rank models for characterizing both global and local trends in traffic time series. Section V and Section VI conduct imputation experiments on real-world traffic time series datasets. In particular, in Section VII, we discuss a possible application of our model to the color image inpainting task and provide a tensor-completion-based approach. Finally, we conclude this study in Section VIII.

## II. RELATED WORK

This section reviews the related work on low-rank matrix/tensor completion. The review consists of two aspects: 1) low-rank matrix/tensor completion models based on special algebraic structures (e.g., circulant matrices and Hankel matrices) and 2) local temporal modeling techniques in matrix/tensor completion.

### A. Low-Rank Completion with Algebraic Structures

Recent studies show great interest in low-rank time series completion models based on certain algebraic structures, e.g., Hankel and circulant matrices. These approaches overcome some limitations of conventional LRMC models, such as being incapable when an entire row/column is missing and invariant to the permutation of rows/columns, or in the case of univariate time series with missing values. For example, the model developed by Yokota et al. [4] can recover the missing slice of tensors using Hankel matrices. Sedighin et al. [13] applied tensor train decomposition to tensors obtained by extended

multi-way delay embedded transform and found better missing data completion performance.

A critical property of a circulant matrix is that its nuclear norm can be efficiently obtained via FFT. Using this property, Yamamoto et al. [5] proposed a fast tensor completion in delay-embedded space; Liu and Zhang [6] used the nuclear norm minimization of circulant matrices for missing data recovery and time series forecasting. Despite the fast algorithm on the circulant matrix, circulant-matrix-based models are inadequate in capturing the local trend/continuity in time series. Therefore, Liu and Zhang [6] proposed a convolution nuclear norm minimization (ConvNNM) model for better local trends modeling. Further, Liu [7] proposed a learnable and orthonormal transformation for ConvNNM to reinforce its modeling ability when the convolutional low-rankness condition is not satisfied.

### B. Imputation with Temporal Modeling

A large body of research has leveraged temporal dynamics in low-rank models for time series imputation. A common assumption among these models is that time series, and thus their low-rank factors, have local smoothness or dependencies.

In terms of local smoothness, Chen and Cichocki [14] proposed a Toeplitz-matrix-based regularizer to impose temporal smoothness in matrix factorization; the regularizer penalizes the difference between the low-rank factors of consecutive time points. A similar regularizer based on the Toeplitz matrix was used by [15] for traffic data reconstruction. Chen et al. [16] applied a quadratic variation minimization term to a traffic tensor completion problem to ensure temporal smoothness.

In terms of modeling temporal dynamics of low-rank factors, Xiong et al. [10] formalized a Bayesian probabilistic tensor factorization with first-order Markovian assumptions on the temporal dimension. Yu et al. [11] developed a temporal autoregressive regularizer in matrix factorization. Chen et al. [17] developed a low-rank autoregressive tensor completion model for traffic data imputation. The above two works assume the independent autoregressive for each latent factor, Chen and Sun [18] applied a vector autoregressive (VAR) model in the latent factors and developed a fully Bayesian solution for multidimensional time series prediction. Chen et al. [12] imposed the VAR process on differenced copy of the temporal factor matrix for nonstationary temporal matrix factorization.

Many studies used Gaussian Process (GP) priors to latent temporal factors for temporal/spatial smoothness [19], [20], i.e., kernelized matrix/tensor factorization. Lei et al. [21] proposed a fully Bayesian solution by an efficient Markov chain Monte Carlo (MCMC) sampling algorithm for kernelized matrix factorization. In fact, the maximum a posteriori (MAP) estimation of using a proper GP prior yields the same form as a Laplacian regularization, where the Laplacian matrix is the inverse of the covariance matrix of the GP prior [22], [20]. As Laplacian regularization is of broad use in graph modeling, it is also applicable to temporal modeling. For example, Rao et al. [23] proposed a scalable collaborative filtering algorithm with spatial and temporal Laplacian regularization for matrix data imputation. To the best of our knowledge, we are the

first to present Laplacian regularization in the form of circular convolution and thus lead to the use of FFT.

### III. PRELIMINARIES

In this section, we first introduce some basic definitions of circulant matrix, convolution matrix, circular convolution, and their relationships. Then, we discuss the existing nuclear norm minimization on the convolution matrix and give a remark on the modeling process of the convolution matrix, circulant matrix, and Hankel matrix.

#### A. Circulant Matrix

In linear algebra, a circulant matrix is an important structure that shows broad use in the field of signal processing [24], [25]. By definition, for any vector  $\mathbf{x} = (x_1, x_2, \dots, x_T)^\top \in \mathbb{R}^T$ , the circulant matrix can be written as

$$\mathcal{C}(\mathbf{x}) \triangleq \begin{bmatrix} x_1 & x_T & x_{T-1} & \cdots & x_2 \\ x_2 & x_1 & x_T & \cdots & x_3 \\ x_3 & x_2 & x_1 & \cdots & x_4 \\ \vdots & \vdots & \vdots & \ddots & \vdots \\ x_T & x_{T-1} & x_{T-2} & \cdots & x_1 \end{bmatrix} \in \mathbb{R}^{T \times T}, \quad (1)$$

where  $\mathcal{C} : \mathbb{R}^T \rightarrow \mathbb{R}^{T \times T}$  denotes the circulant operator. The first column of  $\mathcal{C}(\mathbf{x})$  is the vector  $\mathbf{x}$ , and the diagonal entries of  $\mathcal{C}(\mathbf{x})$  are all about  $x_1$ .

#### B. Convolution Matrix

Convolution is vital to a variety of machine learning problems. By definition, for any vectors  $\mathbf{x} = (x_1, x_2, \dots, x_T)^\top \in \mathbb{R}^T$  and  $\mathbf{y} = (y_1, y_2, \dots, y_\tau)^\top \in \mathbb{R}^\tau$  with  $\tau \leq T$ , the circular convolution of two vectors is  $\mathbf{z} = \mathbf{x} \star \mathbf{y} \in \mathbb{R}^T$  [26], denoting the operator with the symbol  $\star$ ; element-wise, we have

$$z_t = \sum_{k=1}^{\tau} x_{t-k+1} y_k, \quad \forall t \in \{1, 2, \dots, T\}, \quad (2)$$

where  $z_t$  is the  $t$ th entry of  $\mathbf{z}$  and  $x_{t-k+1} = x_{t-k+1+T}$  for  $t+1 \leq k$ . In particular, circular convolution is a linear operator that can be expressed as follows,

$$\mathbf{x} \star \mathbf{y} \equiv \mathcal{C}_\tau(\mathbf{x})\mathbf{y}, \quad (3)$$

where  $\mathcal{C}_\tau : \mathbb{R}^T \rightarrow \mathbb{R}^{T \times \tau}$  denotes the convolution operator and the resultant convolution matrix [6], [7] is given by

$$\mathcal{C}_\tau(\mathbf{x}) \triangleq \begin{bmatrix} x_1 & x_T & x_{T-1} & \cdots & x_{T-\tau+2} \\ x_2 & x_1 & x_T & \cdots & x_{T-\tau+3} \\ x_3 & x_2 & x_1 & \cdots & x_{T-\tau+4} \\ \vdots & \vdots & \vdots & \ddots & \vdots \\ x_T & x_{T-1} & x_{T-2} & \cdots & x_{T-\tau+1} \end{bmatrix} \in \mathbb{R}^{T \times \tau}, \quad (4)$$

where  $\tau$  is the kernel size.

**Remark.** Following Eq. (3), for any  $\mathbf{x} = (x_1, x_2, \dots, x_T)^\top \in \mathbb{R}^T$  and  $\mathbf{y} = (y_1, y_2, \dots, y_T)^\top \in \mathbb{R}^T$  (i.e.,  $\tau = T$ ), then we have the following property:

$$\mathbf{x} \star \mathbf{y} \equiv \mathcal{C}(\mathbf{x})\mathbf{y}, \quad (5)$$

where  $\mathcal{C}(\mathbf{x})$  is the circulant matrix as defined in Eq. (1), showing to be a special case of the convolution matrix.

Essentially, a convolution matrix is a submatrix of the circulant matrix (i.e., the first  $\tau$  columns of the circulant matrix). For any vector  $\mathbf{x} \in \mathbb{R}^T$ , it always holds that

$$\|\mathbf{x}\|_2^2 = \frac{1}{\tau} \|\mathcal{C}_\tau(\mathbf{x})\|_F^2, \quad (6)$$

where  $\|\cdot\|_2$  and  $\|\cdot\|_F$  denote the  $\ell_2$ -norm of a vector and the Frobenius norm of a matrix, respectively.

Unlike the convolution operator, suppose  $\mathcal{H}_\tau : \mathbb{R}^T \rightarrow \mathbb{R}^{(T-\tau+1) \times \tau}$  denotes the Hankel operator [5], then

$$\|\mathbf{x}\|_2^2 \not\propto \|\mathcal{H}_\tau(\mathbf{x})\|_F^2, \quad (7)$$

and it seems that Hankel structure cannot preserve the consistency between data and its Hankelization.

According to the property of the convolution matrix, ConvNNM can be converted into a standard nuclear norm minimization with singular value thresholding [3], [2], [27], [6], [7]. However, unlike the CircNNM problem, it is hard to utilize the property of the convolution matrix to develop fast algorithms through FFT, making the model memory-consuming in real-world applications [6]. In contrast to ConvNNM, CircNNM has an efficient solution through FFT and shows better generalization to high-dimensional data [7].

### IV. METHODOLOGY

In this section, we introduce an LCR model for imputing sparse traffic time series. The cornerstone of LCR includes the definition of the Laplacian kernel. To resolve the involved optimization problem, we seek a fast implementation through FFT in the frequency domain, instead of the time domain.

#### A. Laplacian Kernel

While graph modeling brings new insights into relational data analysis and machine learning, we propose to characterize the temporal dependencies of time series through undirected and circulant graphs. Recall that the Laplacian matrix by definition takes  $\mathbf{L} = \mathbf{D} - \mathbf{A}$  in which  $\mathbf{D}$  and  $\mathbf{A}$  are the (diagonal) degree matrix and adjacency matrix, respectively [28]. As exemplified by Fig. 1, the Laplacian matrices of the two graphs are

$$\mathbf{L} = \begin{bmatrix} 2 & -1 & 0 & 0 & -1 \\ -1 & 2 & -1 & 0 & 0 \\ 0 & -1 & 2 & -1 & 0 \\ 0 & 0 & -1 & 2 & -1 \\ -1 & 0 & 0 & -1 & 2 \end{bmatrix}, \quad (8)$$

and

$$\mathbf{L} = \begin{bmatrix} 4 & -1 & -1 & -1 & -1 \\ -1 & 4 & -1 & -1 & -1 \\ -1 & -1 & 4 & -1 & -1 \\ -1 & -1 & -1 & 4 & -1 \\ -1 & -1 & -1 & -1 & 4 \end{bmatrix}, \quad (9)$$

respectively.

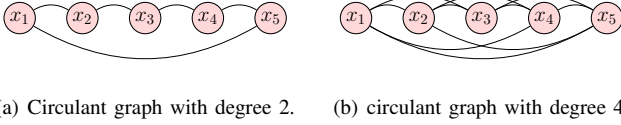


Fig. 1: Undirected and circulant graphs on the relational data samples  $\{x_1, x_2, \dots, x_5\}$  with certain degrees.

Notably, both two Laplacian matrices are circulant matrices, and their first columns are given by  $\ell = (2, -1, 0, 0, -1)^\top$  and  $\ell = (4, -1, -1, -1, -1)^\top$ , respectively.

In this work, we introduce a Laplacian kernel as described in Definition 1, which allows one to encode temporal dependencies of time series. In the aforementioned cases, the first column of the Laplacian matrix  $L$  is indeed a simple example of a Laplacian kernel.

**Definition 1** ((Circular) Laplacian Kernel). *Given any time series  $\mathbf{x} = (x_1, \dots, x_T)^\top \in \mathbb{R}^T$ , suppose  $\tau \in \mathbb{N}^+$  ( $\tau \leq \frac{1}{2}(T-1)$ ) be the kernel size of an undirected and circulant graph, then the Laplacian kernel is defined as*

$$\ell \triangleq (2\tau, \underbrace{-1, \dots, -1}_\tau, 0, \dots, 0, \underbrace{-1, \dots, -1}_\tau)^\top \in \mathbb{R}^T, \quad (10)$$

which is also the first column of the Laplacian matrix and the inherent degree matrix is diagonalized with entries  $2\tau$ .

**Remark.** Here, it is possible to define the Laplacian kernel as a kind of dictionary in the convolutional representation [29], [30], [31] for temporal modeling. As a special case, if we consider the directed and circulant graphs in Fig. 1, then the Laplacian kernels would be  $\ell = (1, 0, 0, 0, -1)^\top$  and  $\ell = (2, 0, 0, -1, -1)^\top$ , respectively. In fact, this case leads to the temporal regularization in the form of random walk [10], which can be demonstrated to reinforce the local trends in time series reconstruction.

Essentially, according to Definition 1, the corresponding Laplacian matrix  $L \in \mathbb{R}^{T \times T}$  can be characterized as a circulant matrix. Recall that the temporal regularization through Laplacian matrix [8] is given by

$$\mathcal{R}_\tau(\mathbf{x}) = \frac{1}{2} \|L\mathbf{x}\|_2^2 = \frac{1}{2} \sum_{i=1}^T \left( \sum_{j \in \Phi(i)} (x_i - x_j) \right)^2, \quad (11)$$

where  $\Phi(i)$  is a set of adjacent nodes of  $x_i$  in the graph. The temporal regularization calculates how values of  $\mathbf{x}$  differ from their adjacent values, and can thus be used as a measure/regularization of local temporal smoothness. According to the definitions of Laplacian kernel and circulant matrix (see Eq. (1)) and the relationship between circular convolution and circulant matrix (see Eq. (5)), we have

$$\mathcal{R}_\tau(\mathbf{x}) = \frac{1}{2} \|\mathcal{C}(\ell)\mathbf{x}\|_2^2 = \frac{1}{2} \|\ell \star \mathbf{x}\|_2^2. \quad (12)$$

In what follows, we utilize the Convolution Theorem (see Theorem 1) to reformulate the temporal regularization in the frequency domain.

**Theorem 1** (Convolution Theorem [26]). *For any vectors  $\mathbf{x}, \mathbf{y} \in \mathbb{R}^T$ , a circular convolution in the time domain is a product in the frequency domain, formally, it always holds that*

$$\mathbf{x} \star \mathbf{y} = \mathcal{F}^{-1}(\mathcal{F}(\mathbf{x}) \circ \mathcal{F}(\mathbf{y})), \quad (13)$$

where  $\mathcal{F}(\cdot)$  and  $\mathcal{F}^{-1}(\cdot)$  denote the discrete Fourier transform and the inverse discrete Fourier transform, respectively.  $\mathcal{F}(\mathbf{x}), \mathcal{F}(\mathbf{y}) \in \mathbb{C}^T$  are the results of discrete Fourier transform on  $\mathbf{x}, \mathbf{y}$  with  $\mathbb{C}$  denoting the set of complex numbers. The symbol  $\circ$  denotes the Hadamard product.

Typically, Theorem 1 gives a concise description of relationship between circular convolution and discrete Fourier transform, and it shows that circular convolution can be implemented in the frequency domain. Circulant matrix is advantageous because the required matrix-vector product can usually be done efficiently by leveraging the structure. Since the Laplacian kernel in this case holds the property of circulant matrix (see Eq. (5)), the temporal regularization in Eq. (11) can be therefore reformulated as follows,

$$\mathcal{R}_\tau(\mathbf{x}) = \frac{1}{2} \|\ell \star \mathbf{x}\|_2^2 = \frac{1}{2T} \|\mathcal{F}(\ell) \circ \mathcal{F}(\mathbf{x})\|_2^2. \quad (14)$$

As can be seen, the temporal regularization through Laplacian matrix is converted into the formula that associated with the Laplacian kernel in the frequency domain. It seems that the length- $T$  Laplacian kernel  $\ell$  can represent the graphical relationship of  $T$ -by- $T$  Laplacian matrix  $L$  in the temporal regularization, showing no need for constructing  $L$ . In the temporal regularization, the coefficients are governed by the Laplacian kernel.

**Remark.** For Eq. (14), we can prove the statement as follows. Let

$$\begin{cases} \alpha = \ell \star \mathbf{x}, \\ \beta = \mathcal{F}(\ell) \circ \mathcal{F}(\mathbf{x}), \end{cases} \quad (15)$$

then it always holds that

$$\alpha = \mathcal{F}^{-1}(\beta) \quad \text{or} \quad \mathcal{F}(\alpha) = \beta. \quad (16)$$

Furthermore, according to the Parseval's theorem [26], we get

$$\|\alpha\|_2^2 = \frac{1}{T} \|\mathcal{F}(\alpha)\|_2^2 = \frac{1}{T} \|\beta\|_2^2, \quad (17)$$

as claimed in Eq. (14).

## B. Univariate Time Series Imputation

Spatiotemporal traffic data modeling is of particular interest to many real-world ITS applications. Typically, traffic flow data by nature involve certain time series characteristics, e.g., global daily/weekly rhythm and local trends. However, such kind of time series are usually incomplete or even sparse due to unpredictable data collection processes. In the univariate case, the imputation problem can be summarized as Problem 1.

**Problem 1** (Univariate Time Series Imputation). *For any partially observed time series  $\mathbf{y} \in \mathbb{R}^T$  with observed index set  $\Omega$ , the goal is to reconstruct the missing values, namely,  $\mathcal{P}_\Omega^\perp(\mathbf{y})$ , from the partial observations  $\mathcal{P}_\Omega(\mathbf{y})$ . Herein,  $\mathcal{P}_\Omega : \mathbb{R}^T \rightarrow \mathbb{R}^T$*

denotes the orthogonal projection supported on the observed index set  $\Omega$ , while  $\mathcal{P}_\Omega^\perp : \mathbb{R}^T \rightarrow \mathbb{R}^T$  denotes the orthogonal projection supported on the complement of  $\Omega$ .

**Remark.** On the vector  $\mathbf{y} \in \mathbb{R}^T$  with observed index set  $\Omega$ , the operator  $\mathcal{P}_\Omega(\cdot)$  can be described as follows,

$$[\mathcal{P}_\Omega(\mathbf{y})]_t = \begin{cases} y_t, & \text{if } t \in \Omega, \\ 0, & \text{otherwise,} \end{cases} \quad (18)$$

where  $t = 1, 2, \dots, T$ .

Although ConvNNM and CircNNM can reconstruct missing values in time series, both two models fail to incorporate both global and local consistency. In this work, we propose a low-rank completion model, i.e., LCR, in which we utilize circulant matrix nuclear norm to pursue the global trends and use the temporal regularization via Laplacian kernel to characterize the local trends in time series (see Fig. 2 for an illustration). Formally, the LCR model can be formulated as follows,

$$\begin{aligned} \min_{\mathbf{x}} \quad & \|\mathcal{C}(\mathbf{x})\|_* + \gamma \cdot \mathcal{R}_\tau(\mathbf{x}) \\ \text{s.t.} \quad & \mathcal{P}_\Omega(\mathbf{x}) = \mathcal{P}_\Omega(\mathbf{y}), \end{aligned} \quad (19)$$

where the notation  $\|\cdot\|_*$  denotes the nuclear norm of matrix, which is defined as the sum of singular values of matrix. The vector  $\mathbf{x} \in \mathbb{R}^T$  is the reconstructed time series corresponding to the partially observed time series  $\mathbf{y}$ . In the objective,  $\gamma$  is the weight parameter.

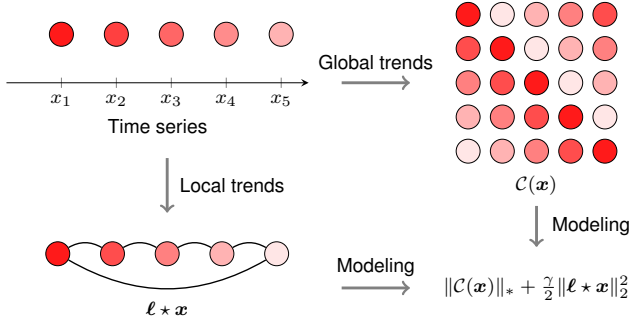


Fig. 2: Illustration of the proposed LCR model.

Since spatiotemporal traffic data are usually noisy, the strong observation constraint in Eq. (19) should be replaced by  $\|\mathcal{P}_\Omega(\mathbf{z} - \mathbf{y})\|_2 \leq \epsilon$  in which  $\epsilon \geq 0$  is the tolerance. Now, the optimization problem of LCR is given by

$$\begin{aligned} \min_{\mathbf{x}} \quad & \|\mathcal{C}(\mathbf{x})\|_* + \gamma \cdot \mathcal{R}_\tau(\mathbf{x}) \\ \text{s.t.} \quad & \|\mathcal{P}_\Omega(\mathbf{x} - \mathbf{y})\|_2 \leq \epsilon. \end{aligned} \quad (20)$$

Our LCR model stems from ConvNNM [6], [7], and it can be solved by the ADMM framework. To resolve the convex optimization problem of LCR in Eq. (20), we introduce an auxiliary variable  $\mathbf{z}$  to preserve the observation information. Thus, the optimization problem now becomes

$$\begin{aligned} \min_{\mathbf{x}, \mathbf{z}} \quad & \|\mathcal{C}(\mathbf{x})\|_* + \gamma \cdot \mathcal{R}_\tau(\mathbf{x}) + \eta \cdot \pi(\mathbf{z}) \\ \text{s.t.} \quad & \mathbf{x} = \mathbf{z}, \end{aligned} \quad (21)$$

where  $\eta$  is the weight parameter. We define  $\pi(\cdot)$  corresponding to the reconstructed errors between  $\mathbf{z}$  and  $\mathbf{y}$  in the set  $\Omega$ , which is given by

$$\pi(\mathbf{z}) = \frac{1}{2} \|\mathcal{P}_\Omega(\mathbf{z} - \mathbf{y})\|_2^2, \quad (22)$$

To reinforce both global and local trends in the reconstructed time series, the observation constraint can be related to the noisy version as shown in Eq. (20), thus leading to the denoised and smooth time series in  $\mathbf{x}$ .

Accordingly, the augmented Lagrangian function of Eq. (21) can be written as follows,

$$\begin{aligned} \mathcal{L}(\mathbf{x}, \mathbf{z}, \mathbf{w}) = & \|\mathcal{C}(\mathbf{x})\|_* + \gamma \cdot \mathcal{R}_\tau(\mathbf{x}) + \frac{\lambda}{2} \|\mathbf{x} - \mathbf{z}\|_2^2 \\ & + \langle \mathbf{w}, \mathbf{x} - \mathbf{z} \rangle + \eta \cdot \pi(\mathbf{z}), \end{aligned} \quad (23)$$

where  $\mathbf{w} \in \mathbb{R}^T$  is the Lagrange multiplier, and  $\lambda$  is the hyperparameter. The symbol  $\langle \cdot, \cdot \rangle$  denotes the inner product. Note that the constraint  $\mathbf{x} = \mathbf{z}$  in the optimization problem is relaxed by the Lagrange multiplier.

Thus, the ADMM scheme can be summarized as follows,

$$\begin{cases} \mathbf{x} := \arg \min_{\mathbf{x}} \mathcal{L}(\mathbf{x}, \mathbf{z}, \mathbf{w}), \\ \mathbf{z} := \arg \min_{\mathbf{z}} \mathcal{L}(\mathbf{x}, \mathbf{z}, \mathbf{w}), \\ \mathbf{w} := \mathbf{w} + \lambda(\mathbf{x} - \mathbf{z}). \end{cases} \quad (24)$$

In particular, with respect to the variable  $\mathbf{x}$ , if we rewrite the regularization terms in Eq. (24) as follows,

$$f = \gamma \cdot \mathcal{R}_\tau(\mathbf{x}) + \frac{\lambda}{2} \|\mathbf{x} - \mathbf{z} + \mathbf{w}/\lambda\|_2^2, \quad (25)$$

then the formula for  $\mathcal{R}_\tau(\mathbf{x})$  can be converted into a discrete Fourier transform copy (see Eq. (14)), and the Parseval's theorem is applicable to the remaining term of  $f$ . Thus, the above formula for  $f$  is equivalent to

$$\begin{aligned} f &= \frac{\gamma}{2} \|\mathcal{L} \star \mathbf{x}\|_2^2 + \frac{\lambda}{2} \|\mathbf{x} - \mathbf{z} + \mathbf{w}/\lambda\|_2^2 \\ &= \frac{\gamma}{2T} \|\mathcal{F}(\mathcal{L}) \circ \mathcal{F}(\mathbf{x})\|_2^2 + \frac{\lambda}{2T} \|\mathcal{F}(\mathbf{x} - \mathbf{z} + \mathbf{w}/\lambda)\|_2^2 \\ &= \frac{\gamma}{2T} \|\hat{\mathcal{L}} \circ \hat{\mathbf{x}}\|_2^2 + \frac{\lambda}{2T} \|\hat{\mathbf{x}} - \hat{\mathbf{z}} + \hat{\mathbf{w}}/\lambda\|_2^2, \end{aligned} \quad (26)$$

where  $\hat{\mathcal{L}} = \mathcal{F}(\mathcal{L})$ , and we introduce the variables  $\{\hat{\mathbf{x}}, \hat{\mathbf{z}}, \hat{\mathbf{w}}\} = \{\mathcal{F}(\mathbf{x}), \mathcal{F}(\mathbf{z}), \mathcal{F}(\mathbf{w})\}$  referring to the variables  $\{\mathbf{x}, \mathbf{z}, \mathbf{w}\}$  in the frequency domain.

Accordingly, the partial derivative of the function  $f$  with respect to the variable  $\hat{\mathbf{x}}$  is given by

$$\begin{aligned} \frac{\partial f}{\partial \hat{\mathbf{x}}} &= \frac{\gamma}{T} \hat{\mathcal{L}} \circ \hat{\mathbf{x}} + \frac{\lambda}{T} (\hat{\mathbf{x}} - \hat{\mathbf{z}} + \hat{\mathbf{w}}/\lambda) \\ &= \frac{1}{T} (\gamma \hat{\mathcal{L}} \circ \hat{\mathbf{x}} + \lambda \mathbb{1}_T) \circ \hat{\mathbf{x}} - \frac{1}{T} (\lambda \hat{\mathbf{z}} - \hat{\mathbf{w}}), \end{aligned} \quad (27)$$

where  $\mathbb{1}_T \in \mathbb{R}^T$  is the vector comprised of ones.

Let  $\frac{\partial f}{\partial \hat{\mathbf{x}}} = \mathbf{0}$ , then it produces a closed-form solution such that

$$\hat{\mathbf{x}} = (\lambda \hat{\mathbf{z}} - \hat{\mathbf{w}}) \oslash (\gamma \hat{\mathcal{L}} \circ \hat{\mathbf{x}} + \lambda \mathbb{1}_T), \quad (28)$$

where  $\oslash$  denotes the Hadamard division.

Going back to the ADMM scheme, the subproblem for optimizing the variable  $\mathbf{x}$  in the time domain can be converted

into the optimization over the variable  $\hat{\mathbf{x}}$  in the frequency domain, i.e.,

$$\hat{\mathbf{x}} := \arg \min_{\hat{\mathbf{x}}} \|\hat{\mathbf{x}}\|_1 + \frac{\lambda}{2T} \|\hat{\mathbf{x}} - (\lambda \hat{\mathbf{z}} - \hat{\mathbf{w}}) \odot (\gamma \hat{\ell} \circ \hat{\ell} + \lambda \mathbb{1}_T)\|_2^2. \quad (29)$$

The resultant  $\ell_1$ -norm minimization is memory efficient, easy to compute with, and preserves the singular values of circulant matrix that are due to the discrete Fourier transform.

**Lemma 1.** *For any vector  $\mathbf{x} \in \mathbb{R}^T$ , the nuclear norm of the resultant circulant matrix  $\mathcal{C}(\mathbf{x}) \in \mathbb{R}^{T \times T}$  is related to the discrete Fourier transform:*

$$\|\mathcal{C}(\mathbf{x})\|_* = \|\mathcal{F}(\mathbf{x})\|_1. \quad (30)$$

*Proof.* For any circulant matrix  $\mathcal{C}(\mathbf{x})$  if and only if it is diagonalizable by the unitary matrix, the eigenvalue decomposition [25] can be written as follows,

$$\mathcal{C}(\mathbf{x}) = \mathbf{U} \text{diag}(\mathcal{F}(\mathbf{x})) \mathbf{U}^H, \quad (31)$$

where  $\cdot^H$  denotes the conjugate transpose. Since  $\mathbf{U}$  is a unitary matrix, it always holds that

$$\begin{aligned} \|\mathcal{C}(\mathbf{x})\|_* &= \|\mathbf{U} \text{diag}(\mathcal{F}(\mathbf{x})) \mathbf{U}^H\|_* \\ &= \|\text{diag}(\mathcal{F}(\mathbf{x}))\|_* \\ &= \|\mathcal{F}(\mathbf{x})\|_1, \end{aligned} \quad (32)$$

and we can quickly calculate the singular values of  $\mathcal{C}(\mathbf{x})$  from the FFT of  $\mathbf{x}$ , i.e.,  $\mathcal{F}(\mathbf{x})$ . Typically, FFT is an efficient algorithm for computing the discrete Fourier transform in  $\mathcal{O}(T \log T)$  time.  $\square$

In Eq. (29), let

$$\hat{\mathbf{h}} \triangleq (\lambda \hat{\mathbf{z}} - \hat{\mathbf{w}}) \odot (\gamma \hat{\ell} \circ \hat{\ell} + \lambda \mathbb{1}_T), \quad (33)$$

then the closed-form solution to  $\hat{\mathbf{x}}$  can be found in Lemma 2. As we have the closed-form solution as described in Eq. (36) in the frequency domain, we can update the variable  $\mathbf{x}$  by

$$\mathbf{x} := \mathcal{F}^{-1}(\hat{\mathbf{x}}). \quad (34)$$

**Lemma 2.** *Following Eq. (29), for any optimization problem in the form of  $\ell_1$ -norm minimization in complex space, i.e.,*

$$\min_{\hat{\mathbf{x}}} \|\hat{\mathbf{x}}\|_1 + \frac{\lambda}{2T} \|\hat{\mathbf{x}} - \hat{\mathbf{h}}\|_2^2, \quad (35)$$

with complex-valued  $\hat{\mathbf{x}}, \hat{\mathbf{h}} \in \mathbb{C}^T$ , element-wise, the solution is given by

$$\hat{x}_t := \frac{\hat{h}_t}{|\hat{h}_t|} \cdot \max\{0, |\hat{h}_t| - T/\lambda\}, t = 1, \dots, T. \quad (36)$$

*Proof.* In theory, Lemma 2 invokes the shrinkage operator in [32], [33], [6].  $\square$

In the ADMM scheme (see Eq. (24)), the subproblem with respect to the variable  $\mathbf{z}$  can be written as follows,

$$\min_{\mathbf{z}} \frac{\lambda}{2} \|\mathbf{x} - \mathbf{z} - \mathbf{w}/\lambda\|_2^2 + \frac{\eta}{2} \|\mathcal{P}_\Omega(\mathbf{z} - \mathbf{y})\|_2^2, \quad (37)$$

if we let  $g$  be the objective function, then the partial derivative with respect to the variable  $\mathbf{z}$  can be formed by  $\mathcal{P}_\Omega(\mathbf{z})$  and  $\mathcal{P}_\Omega^\perp(\mathbf{z})$ . Here, we have

$$\begin{aligned} \frac{\partial g}{\partial \mathcal{P}_\Omega(\mathbf{z})} &= \lambda \mathcal{P}_\Omega(\mathbf{z} - \mathbf{x} - \mathbf{w}/\lambda) + \eta \mathcal{P}_\Omega(\mathbf{z} - \mathbf{y}), \\ \frac{\partial g}{\partial \mathcal{P}_\Omega^\perp(\mathbf{z})} &= \lambda \mathcal{P}_\Omega^\perp(\mathbf{z} - \mathbf{x} - \mathbf{w}/\lambda). \end{aligned} \quad (38)$$

In what follows,  $\frac{\partial g}{\partial \mathbf{z}} = \mathbf{0}$  allows one to infer a closed-form solution to the variable  $\mathbf{z}$ :

$$\mathbf{z} := \frac{1}{\lambda + \eta} \mathcal{P}_\Omega(\lambda \mathbf{x} + \mathbf{w} + \eta \mathbf{y}) + \mathcal{P}_\Omega^\perp(\mathbf{x} + \mathbf{w}/\lambda). \quad (39)$$

**Remark.** If  $\eta \rightarrow +\infty$ , then the solution would be  $\mathbf{z} := \mathcal{P}_\Omega(\mathbf{y}) + \mathcal{P}_\Omega^\perp(\mathbf{x} + \mathbf{w}/\lambda)$ , corresponding to the LCR model with strong observation constraint in Eq. (19). In terms of the parameter  $\eta$ , we can preferably set the default one as  $\eta = c \cdot \lambda$  with  $c \in \{10^2, 10^3\}$  to preserve the observation information.

As mentioned above, our LCR model bridges the gap between the modeling processes of global low-rank properties and local temporal trends underlying time series data, therefore reinforcing both global and local consistency. Since we utilize circulant matrix and circular Laplacian kernel in our model, it is not hard to show the appealing properties of discrete Fourier transform and lead to an elegant and fast solution algorithm. Algorithm 1 summarizes the implementation of the proposed LCR model.

---

#### Algorithm 1 Laplacian Convolutional Representation (LCR)

---

**Input:** Data  $\mathbf{y} \in \mathbb{R}^T$  with observed index set  $\Omega$ , Laplacian kernel size  $\tau \in \mathbb{N}^+$ , and hyperparameters  $\{\gamma, \lambda, \eta\}$ .

**Output:** Reconstructed vector  $\mathbf{x} \in \mathbb{R}^T$ .

- 1: Initialize  $\{\mathbf{x}_0, \mathbf{z}_0, \mathbf{w}_0\}$ .
  - 2: Construct the Laplacian kernel  $\ell$  with  $\tau$  and perform FFT on it to get  $\hat{\ell}$ .
  - 3: **for**  $i = 0$  to maximum iteration **do**
  - 4:   Perform FFT on  $\{\mathbf{z}_i, \mathbf{w}_i\}$ .
  - 5:   Compute  $\hat{\mathbf{h}}$  by Eq. (33).
  - 6:   Compute  $\hat{\mathbf{x}}$  by the shrinkage in Eq. (36).
  - 7:   Compute  $\mathbf{x}_{i+1}$  by  $\mathbf{x}_{i+1} = \mathcal{F}^{-1}(\hat{\mathbf{x}})$  (see Eq. (34)).
  - 8:   Compute  $\mathbf{z}_{i+1}$  by Eq. (39).
  - 9:   Compute  $\mathbf{w}_{i+1} = \mathbf{w}_i + \lambda(\mathbf{x}_{i+1} - \mathbf{z}_{i+1})$  (see Eq. (24)).
  - 10: **end for**
- 

### C. Multivariate Time Series Imputation

Considering both spatial and temporal dimensions in traffic data, we have a multivariate time series imputation task as described in Problem 2. The critical question is how to characterize both spatial and temporal dependencies of traffic time series data in the modeling process.

**Problem 2** (Multivariate Time Series Imputation). *For any partially observed time series  $\mathbf{Y} \in \mathbb{R}^{N \times T}$  consisting of  $N$  variables and  $T$  time steps, if its observed index set is denoted by  $\Omega$ , then the goal is to reconstruct the missing values, namely,  $\mathcal{P}_\Omega^\perp(\mathbf{Y})$ , from the partial observations  $\mathcal{P}_\Omega(\mathbf{Y})$ .*

Herein,  $\mathcal{P}_\Omega : \mathbb{R}^{N \times T} \rightarrow \mathbb{R}^{N \times T}$  denotes the orthogonal projection supported on the observed index set  $\Omega$ , while  $\mathcal{P}_\Omega^\perp : \mathbb{R}^{N \times T} \rightarrow \mathbb{R}^{N \times T}$  denotes the orthogonal projection supported on the complement of  $\Omega$ .

On the multivariate time series  $\mathbf{Y}$ , the first impulse is to follow the LCR model in the univariate case and formulate the multivariate model as follows,

$$\begin{aligned} \min_{\mathbf{X}} \quad & \|\mathcal{C}(\mathbf{X})\|_* + \frac{\gamma}{2} \|\mathbf{L}\mathbf{X}^\top\|_F^2 \\ \text{s.t.} \quad & \|\mathcal{P}_\Omega(\mathbf{X} - \mathbf{Y})\|_F \leq \epsilon, \end{aligned} \quad (40)$$

where  $\mathbf{L} \in \mathbb{R}^{T \times T}$  is the Laplacian matrix. However, the Laplacian matrix/kernel in the temporal dimension works on each time series independently. If we aim to build the connection between circulant matrix and discrete Fourier transform, then the problem would be reduced to

$$\begin{aligned} \min_{\mathbf{X}} \quad & \sum_{n=1}^N \|\mathcal{C}(x_n)\|_* + \frac{\gamma}{2} \sum_{n=1}^N \|\ell \star x_n\|_2^2 \\ \text{s.t.} \quad & \|\mathcal{P}_\Omega(\mathbf{X} - \mathbf{Y})\|_F \leq \epsilon. \end{aligned} \quad (41)$$

In this case, the whole problem is divided into  $N$  subproblems (defined as  $\text{LCR}_N$  in the following). The reconstruction of multivariate time series is achieved by reconstructing each time series independently.

To jointly characterize the spatial and temporal dependencies for traffic time series, we consider a separable kernel in the LCR model, namely,

$$\mathbf{K} \triangleq \ell_s \ell^\top \in \mathbb{R}^{N \times T}, \quad (42)$$

with the spatial kernel  $\ell_s = (1, 0, \dots, 0)^\top \in \mathbb{R}^N$  (i.e., the first column of the  $N$ -by- $N$  identity matrix). The optimization problem of two-dimensional LCR (LCR-2D) can be formulated as follows,

$$\begin{aligned} \min_{\mathbf{X}} \quad & \|\mathcal{C}(\mathbf{X})\|_* + \frac{\gamma}{2} \|\mathbf{K} \star \mathbf{X}\|_F^2 \\ \text{s.t.} \quad & \|\mathcal{P}_\Omega(\mathbf{X} - \mathbf{Y})\|_F \leq \epsilon, \end{aligned} \quad (43)$$

where the two-dimensional (2D) circular convolution is described in Definition 2. Although the spatial kernel  $\ell_s$  does not provide any spatial dependencies, the nuclear norm of circulant operator on  $\mathbf{X}$  can give implicit spatial modeling.

**Definition 2** (2D Circular Convolution [34], [24]). For any matrices  $\mathbf{X} \in \mathbb{R}^{N \times T}$  and  $\mathbf{K} \in \mathbb{R}^{\nu_1 \times \nu_2}$  with  $\nu_1 \leq N, \nu_2 \leq T$ , the circular convolution of two matrices is

$$\mathbf{Z} = \mathbf{K} \star \mathbf{X} \in \mathbb{R}^{N \times T}, \quad (44)$$

or element-wise,

$$z_{n,t} = \sum_{i=1}^{\nu_1} \sum_{j=1}^{\nu_2} \kappa_{i,j} x_{n-i+1, t-j+1}, \quad (45)$$

where  $n = 1, 2, \dots, N$  and  $t = 1, 2, \dots, T$ .  $\kappa_{i,j}$  is the  $(i, j)$ -th entry of  $\mathbf{K}$ . The symbol  $\star$  denotes the operator of convolution.

**Remark.** In the field of signal processing, the 2D circular convolution also shows the properties that associated with

two-dimensional discrete Fourier transform. According to the convolution theorem and the Parseval's theorem, we have

$$\|\mathbf{K} \star \mathbf{X}\|_F^2 = \frac{1}{NT} \|\mathcal{F}(\mathbf{K}) \circ \mathcal{F}(\mathbf{X})\|_F^2, \quad (46)$$

where  $\mathcal{F}(\cdot)$  denotes the 2D discrete Fourier transform. Typically, 2D discrete Fourier transform can be computed by first transforming each column vector (or row vector) of the matrix and then each row vector (or column vector) of the matrix [24].

As mentioned above, LCR in the multivariate case is also a convex problem that can be resolved by the ADMM framework. Following Eq. (24), the ADMM scheme is given by

$$\begin{cases} \mathbf{X} := \arg \min_{\mathbf{X}} \mathcal{L}(\mathbf{X}, \mathbf{Z}, \mathbf{W}), \\ \mathbf{Z} := \arg \min_{\mathbf{Z}} \mathcal{L}(\mathbf{X}, \mathbf{Z}, \mathbf{W}) \\ \quad = \frac{1}{\lambda + \eta} \mathcal{P}_\Omega(\lambda \mathbf{X} + \mathbf{W} + \eta \mathbf{Y}) + \mathcal{P}_\Omega^\perp(\mathbf{X} + \mathbf{W}/\lambda), \\ \mathbf{W} := \mathbf{W} + \lambda(\mathbf{X} - \mathbf{Z}), \end{cases} \quad (47)$$

where  $\mathcal{L}(\mathbf{X}, \mathbf{Z}, \mathbf{W})$  is the augmented Lagrangian function:

$$\begin{aligned} \mathcal{L}(\mathbf{X}, \mathbf{Z}, \mathbf{W}) = & \|\mathcal{C}(\mathbf{X})\|_* + \frac{\gamma}{2} \|\mathbf{K} \star \mathbf{X}\|_F^2 \\ & + \frac{\lambda}{2} \|\mathbf{X} - \mathbf{Z}\|_F^2 + \langle \mathbf{W}, \mathbf{X} - \mathbf{Z} \rangle \\ & + \frac{\eta}{2} \|\mathcal{P}_\Omega(\mathbf{Z} - \mathbf{Y})\|_F^2. \end{aligned} \quad (48)$$

With respect to the variable  $\mathbf{X}$ , the subproblem is

$$\begin{aligned} \mathbf{X} := \arg \min_{\mathbf{X}} \quad & \|\mathcal{C}(\mathbf{X})\|_* + \frac{\gamma}{2} \|\mathbf{K} \star \mathbf{X}\|_F^2 \\ & + \frac{\lambda}{2} \|\mathbf{X} - \mathbf{Z} + \mathbf{W}/\lambda\|_2^2. \end{aligned} \quad (49)$$

Although the nuclear norm of circulant tensor is more complicated than the nuclear norm of circulant matrix as mentioned in Lemma 1, 2D discrete Fourier transform is also applicable for finding the equivalent formula. In the frequency domain, it takes

$$\begin{aligned} \hat{\mathbf{X}} := \arg \min_{\hat{\mathbf{X}}} \quad & \|\hat{\mathbf{X}}\|_1 + \frac{\gamma}{2NT} \|\hat{\mathbf{K}} \circ \hat{\mathbf{X}}\|_F^2 \\ & + \frac{\lambda}{2NT} \|\hat{\mathbf{X}} - \hat{\mathbf{Z}} + \hat{\mathbf{W}}/\lambda\|_F^2, \end{aligned} \quad (50)$$

where we introduce the two-dimensional discrete Fourier transformed  $\{\hat{\mathbf{K}}, \hat{\mathbf{X}}, \hat{\mathbf{Z}}, \hat{\mathbf{W}}\}$  referring to  $\{\mathbf{K}, \mathbf{X}, \mathbf{Z}, \mathbf{W}\}$  in the frequency domain. Without loss of generality, this subproblem for  $\ell_1$ -norm minimization in complex space can also be solved by the shrinkage operator in Eq. (36). Algorithm 2 summarizes the whole scheme of LCR-2D.

## V. UNIVARIATE TRAFFIC TIME SERIES IMPUTATION

This section evaluates the reconstruction of univariate traffic time series from partial observations. The reconstruction results of the proposed LCR model are compared with several baseline models. Experiments are based on traffic speed time series (weak periodicity and strong noises) and traffic volume time series (strong periodicity). We focus on understanding

---

**Algorithm 2** Two-Dimensional Laplacian Convolutional Representation (LCR-2D)

---

**Input:** Data  $\mathbf{Y} \in \mathbb{R}^{N \times T}$  with observed index set  $\Omega$ , Laplacian kernel size  $\tau \in \mathbb{N}^+$ , and hyperparameters  $\{\gamma, \lambda, \eta\}$ .

**Output:** Reconstructed vector  $\mathbf{X} \in \mathbb{R}^{N \times T}$ .

- 1: Initialize  $\{\mathbf{X}_0, \mathbf{Z}_0, \mathbf{W}_0\}$ .
  - 2: Construct the Laplacian kernel  $\ell \in \mathbb{R}^T$  with  $\tau$ .
  - 3: Construct the spatial kernel  $\ell_s = (1, 0, \dots, 0) \in \mathbb{R}^N$  and build up a separable kernel  $\mathbf{K} \triangleq \ell_s \ell^\top$ .
  - 4: **for**  $i = 0$  to maximum iteration **do**
  - 5:   Perform FFT on  $\{\mathbf{Z}_i, \mathbf{W}_i\}$ .
  - 6:   Compute  $\hat{\mathbf{X}}$  by referring to the shrinkage in Eq. (36).
  - 7:   Compute  $\mathbf{X}_{i+1}$  by  $\mathbf{X}_{i+1} = \mathcal{F}^{-1}(\hat{\mathbf{X}})$ .
  - 8:   Compute  $\mathbf{Z}_{i+1}$  by Eq. (47).
  - 9:   Compute  $\mathbf{W}_{i+1}$  by Eq. (47).
  - 10: **end for**
- 

how well the reconstructed time series preserve the global and local trends of the ground truth time series in the imputation task. The adapted datasets and Python implementation are publicly available at <https://github.com/xinychen/transdim>.

#### A. Traffic Speed

We begin with some preliminary experiments on univariate freeway traffic speed time series collected through dual-loop detectors in Portland, USA.<sup>1</sup> The speed observations have 15-min time resolution (i.e., 96 expected data samples per day) over three days, and the data vector is of length 288. In particular, we consider the imputation scenarios on fully observed, 50%, 20%, 10%, and 5% observed data, respectively. To generate the partially observed time series, we randomly mask a certain number of observations as missing values.

Fig. 3 shows the reconstruction/imputation results produced by our LCR model. Fig. 3(a) demonstrates the reconstructed time series by LCR on the fully observed time series, in which the data noises can be smoothed out due to the existence of Laplacian temporal regularization and the relaxation of observation constraint in the ADMM scheme (see Eq. (24)). Fig. 3(b), 3(c), and 3(d) show the imputation performance by LCR with partial observations. Of these results, the reconstructed time series can accurately approximate both partial observations and missing values while preserving the trends of the ground truth time series.

Next, we test a more challenging scenario in which we aim to reconstruct 95% missing values from 5% observations (i.e., reconstructing 274 missing values from only 14 data samples). We compare the time series imputation of LCR with the following baseline models:

- CircNNM [6]. This is a fast implementation of nuclear norm minimization on the circulant matrix via FFT, which can be regarded as a special case of our LCR model without temporal regularization.
- ConvNNM [6]. This is a standard nuclear norm minimization method on the convolution matrix.

<sup>1</sup><https://portal.its.pdx.edu/>

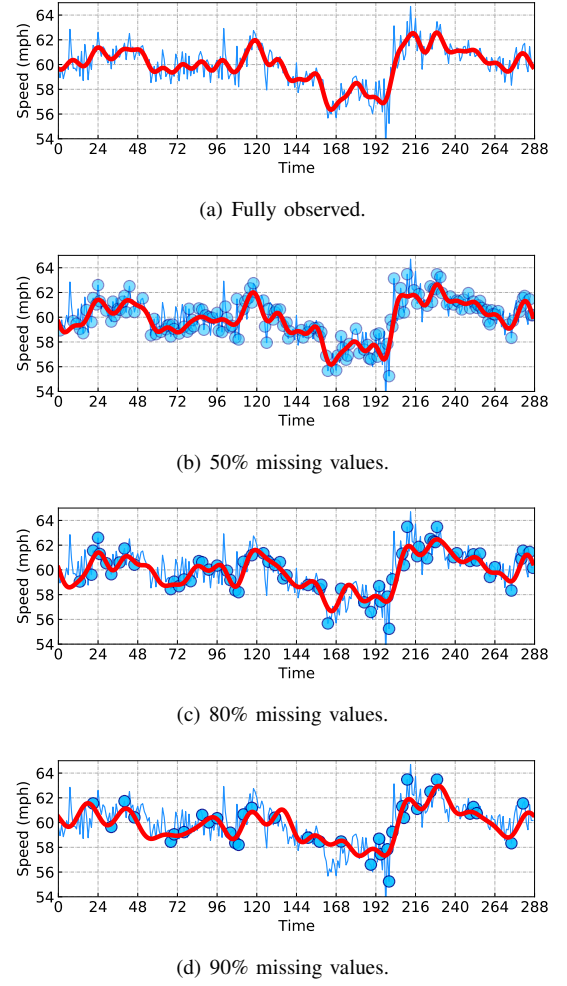


Fig. 3: Univariate traffic time series imputation on the freeway traffic speed time series. The blue curve represents the ground truth time series, while the red curve refers to the reconstructed time series produced by LCR. Here, partial observations are illustrated as blue circles.

- Gaussian process (GP, [35]). The GP regression model with a squared exponential kernel. The hyperparameters are optimized via the maximum marginal likelihood method.

The imputation results on the given traffic speed time series are shown in Fig. 4, we can summarize the following findings for the baseline models:

- The reconstructed time series by CircNNM shows high fluctuations due to the lack of Laplacian temporal regularization. As a result, the reconstructed time series fails to reproduce trends of the ground truth time series under such a high missing rate.
- ConvNNM performs better than CircNNM. The reconstructed time series fits the observed values well, but the trend is still far from the ground truth time series. Unlike CircNNM, ConvNNM cannot employ a fast implementation through FFT. As a result, ConvNNM is not scalable to large problems.
- The GP model reasonably reconstructs the traffic speed

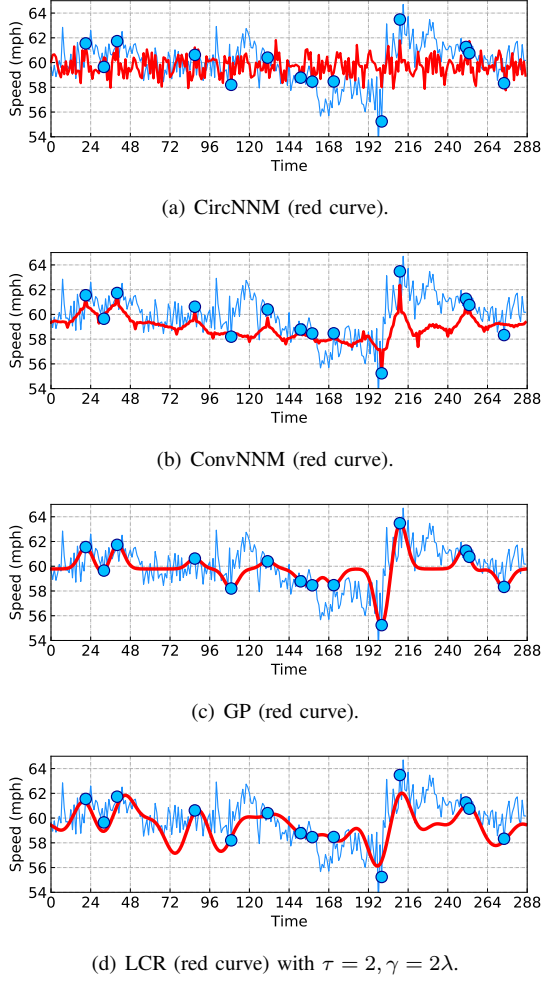


Fig. 4: Univariate traffic time series imputation on the freeway traffic speed time series. In this case, we mask 95% observations as missing values and only have 14 speed observations for training the model.

time series, but has a huge computational cost. A common fact is that GP models are not well-suited to long time series and large problems due to their high time complexity of  $\mathcal{O}(T^3)$ .

As shown in Fig. 4(d), the reconstructed time series by LCR demonstrates consistent global and local trends with the trends of ground truth time series, and our LCR model clearly outperforms the baseline models in terms of either accuracy or computational efficiency. By comparing CircNNM with LCR, the imputation results emphasize the importance of temporal regularization with Laplacian kernel. In terms of temporal modeling, the proposed temporal regularization via Laplacian kernel presents an FFT solution in  $\mathcal{O}(T \log T)$  time, which is much more computationally efficient than GP with  $\mathcal{O}(T^3)$  time.

### B. Traffic Volume

In addition to the traffic speed time series, we evaluate the model on the freeway traffic volume time series collected

through loop detectors in Portland, USA. The volume observations are with 15-min time resolution over three days, and the data vector is of length 288. The time series is characterized by a strong daily rhythm (see Fig. 5). The time series shows relatively low traffic volume at night, and the traffic volume reaches a peak during rush hours, demonstrating typical traveler’s behavioral rhythms. As shown in Fig. 5, the time series possesses strong seasonality and three remarkable peaks over three days.

The task is reconstructing 95% missing values from 5% observations. As can be seen, due to the lack of explicit temporal modeling, both CircNNM and ConvNNM models cannot produce smooth time series as LCR. Observing the reconstructed time series, it is clear that LCR produces much more accurate reconstruction results than both CircNNM and ConvNNM. Yet, on the contrary to the traffic speed time series, due to the strong seasonality (i.e., daily rhythm in traffic flow) in the traffic volume time series, both CircNNM and ConvNNM can produce reasonable time series, which seems to be consistent with the results in [7].

## VI. MULTIVARIATE TRAFFIC TIME SERIES IMPUTATION

In what follows, we study the generalization of LCR to high-dimensional data and evaluate the model on a large-scale traffic flow dataset. The data are collected by the California department of transportation through their Performance Measurement System (PeMS) [36]. This dataset contains freeway traffic speed collected from 11,160 traffic measurement sensors over 4 weeks (the first 4 weeks in the year of 2018) with a 5-minute time resolution (288 time intervals per day) in California, USA.<sup>2</sup> It can be arranged in a matrix of size  $11160 \times 8064$ . Note that this dataset contains about 90 million observations; many existing methods, such as GP, are not applicable to such a large-scale dataset.

To set up the imputation task, we randomly mask 30%, 50%, 70%, and 90% traffic speed observations as missing values, referred to as 30%, 50%, 70%, and 90% missing rates, respectively. To assess the imputation performance, we use the actual values of the masked missing entries as the ground truth to compute the mean absolute percentage error (MAPE) and root mean square error (RMSE):

$$\text{MAPE} = \frac{1}{n} \sum_{i=1}^n \frac{|y_i - \hat{y}_i|}{y_i} \times 100,$$

$$\text{RMSE} = \sqrt{\frac{1}{n} \sum_{i=1}^n (y_i - \hat{y}_i)^2},$$

where  $n$  is the total number of estimated values, and  $y_i$  and  $\hat{y}_i$  are the actual value and its estimation, respectively.

For the comparisons, we choose the baseline models as CircNNM [6], LRMC [3], and nonstationary temporal matrix factorization (NoTMF [12]). Through cross validation, we have the following hyperparameter settings:

- LCR-2D: We set the hyperparameters as  $\lambda = 1 \times 10^{-5} NT$ ,  $\eta = 10^2 \lambda$ , and  $\gamma = 5 \lambda$ .

<sup>2</sup>The dataset is available at <https://doi.org/10.5281/zenodo.3939792>.

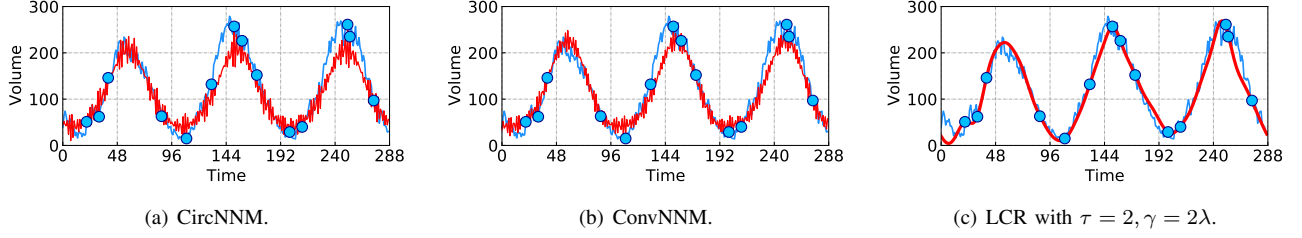


Fig. 5: Univariate time series imputation on the freeway traffic volume time series. In this case, we randomly remove 95% observations as missing values, and we only have 14 volume observations for the reconstruction.

- LCR<sub>N</sub>: We set the hyperparameters as  $\lambda = 5 \times 10^{-3}T$  and  $\eta = 10^3\lambda$ ; since LCR is accomplished over  $N$  subproblems independently, we set  $\gamma = 5\lambda$  at all missing rates for seeking better local trends.
- LCR: We consider the LCR via the vectorization on the multivariate time series [7], which is given by

$$\begin{aligned} \min_{\mathbf{X}} \quad & \|\mathcal{C}(\text{vec}(\mathbf{X}^\top))\|_* + \frac{\gamma}{2} \|\ell \star \text{vec}(\mathbf{X}^\top)\|_2^2 \\ \text{s.t.} \quad & \|\mathcal{P}_\Omega(\mathbf{X} - \mathbf{Y})\|_F \leq \epsilon, \end{aligned} \quad (51)$$

where  $\text{vec}(\cdot)$  denotes the operator of vectorization. The Laplacian kernel  $\ell$  is of length  $NT$ . We set the hyperparameters as  $\lambda = 5 \times 10^{-6}NT$ ,  $\eta = 10^2\lambda$ , and  $\gamma = 5\lambda$ .

- CircNNM: We follow the nuclear norm minimization of circulant matrix via the vectorization [6] and set the hyperparameters as  $\lambda = 5 \times 10^{-7}NT$  and  $\eta = 10^2\lambda$ .

Notably, to assess the importance of local temporal modeling thoroughly, we evaluate the LCR models with different Laplacian kernels parameterized by  $\tau = 1, 2, 3$ . From Table I, in the case of a relatively small missing rate (e.g., 30%), LCR-2D, LCR<sub>N</sub>, and LCR perform best with the kernel size  $\tau = 1$ . However, when the missing rate reaches 90%, setting the kernel size as  $\tau = 2, 3$  in the LCR models can produce more competitive results. These demonstrate the importance of a proper Laplacian kernel for characterizing the local trends in time series. When learning LCR from limited observations with a relatively high missing rate, local trend modeling in LCR demands more informative Laplacian kernels.

Among the baseline models in Table I, CircNNM can be implemented by FFT, which is a special case of our LCR model without the temporal regularization. By comparing the performance of CircNNM and LCR, we can find the significant improvement of imputation achieved by LCR over CircNNM, mainly due to the existence of the temporal regularization. Moreover, our LCR models significantly outperform LRMC and NoTMF. Here, LRMC provides a well-suited framework for reconstructing incomplete matrix, however, it involves high time complexity in the process of singular value thresholding, making it extremely costly to work on the large-scale problems. NoTMF jointly models global and local trends by a unified and efficient temporal matrix factorization framework, but as can be seen, it is inferior to the LCR models.

Notably, since this work takes the same experiment settings on the PeMS-4W dataset as [16], our LCR models also perform better than the state-of-the-art low-rank tensor completion models. Beyond the matrix/tensor completion models

TABLE I: Imputation performance (MAPE/RMSE) on the PeMS-4W traffic speed dataset. Note that the best results are highlighted in bold fonts.

Missing rate	30%	50%	70%	90%
LCR-2D ( $\tau = 1$ )	1.57/1.54	1.81/1.74	2.29/2.12	3.80/3.17
LCR-2D ( $\tau = 2$ )	1.74/1.70	1.89/1.84	2.21/2.15	3.40/3.07
LCR-2D ( $\tau = 3$ )	2.00/1.94	2.12/2.06	2.37/2.31	3.32/3.13
LCR <sub>N</sub> ( $\tau = 1$ )	<b>1.51/1.53</b>	<b>1.73/1.76</b>	2.18/2.19	3.77/3.49
LCR <sub>N</sub> ( $\tau = 2$ )	1.70/1.69	1.84/1.85	<b>2.15/2.19</b>	3.32/3.28
LCR <sub>N</sub> ( $\tau = 3$ )	1.99/1.96	2.11/2.09	2.35/2.35	<b>3.30/3.32</b>
LCR ( $\tau = 1$ )	1.60/1.55	1.82/ <b>1.73</b>	2.29/ <b>2.10</b>	3.86/3.18
LCR ( $\tau = 2$ )	1.83/1.77	1.97/1.90	2.28/2.17	3.47/ <b>3.05</b>
LCR ( $\tau = 3$ )	2.11/2.03	2.23/2.14	2.47/2.37	3.41/3.11
CircNNM	2.41/2.03	2.80/2.33	3.48/2.82	5.22/4.03
LRMC	2.04/1.80	2.43/2.12	3.08/2.66	6.05/4.43
NoTMF	2.95/2.65	3.05/2.73	3.33/2.97	5.22/4.71

that employ the costly process of singular value thresholding, our LCR models convert the nuclear norm minimization problem as an  $\ell_1$ -norm minimization problem in the frequency domain. It seems that LCR is a well-suited framework for both univariate and multivariate time series imputation of various data scales.

Fig. 6 shows the speed imputation results of three road segments under 70% and 90% missing rates. Despite the high missing rates, we can see that the reconstructed curves of LCR preserve the overall trend of the original speed time series. Notably, the reconstructed curves even correctly depict the sharp decrease of the speed during congestion periods, demonstrating the effectiveness of LCR in capturing local information of the traffic speed time series.

## VII. DISCUSSION: APPLICATION TO IMAGE INPAINTING

In fact, the basic idea of Laplacian regularization in LCR also applies to more general imputation problems like image inpainting, i.e., reconstructing missing regions/pixels in an image (e.g., Problem 3). In this task, we can verify the importance of local (spatial) modeling via the use of the Laplacian kernel as described in Definition 1.

**Problem 3** (Color Image Inpainting). *For any (RGB) color image  $\mathcal{Y} \in \mathbb{R}^{M \times N \times 3}$  consisting of  $M$  rows and  $N$  columns with three RGB channels, if its observed index set is denoted by  $\Omega$ , then the goal is to reconstruct missing values  $\mathcal{P}_\Omega^\perp(\mathcal{Y})$  from the partial observations  $\mathcal{P}_\Omega(\mathcal{Y})$ .*

In this case, we consider to explicitly establish the local correlations for the rows/columns of an image via the use of

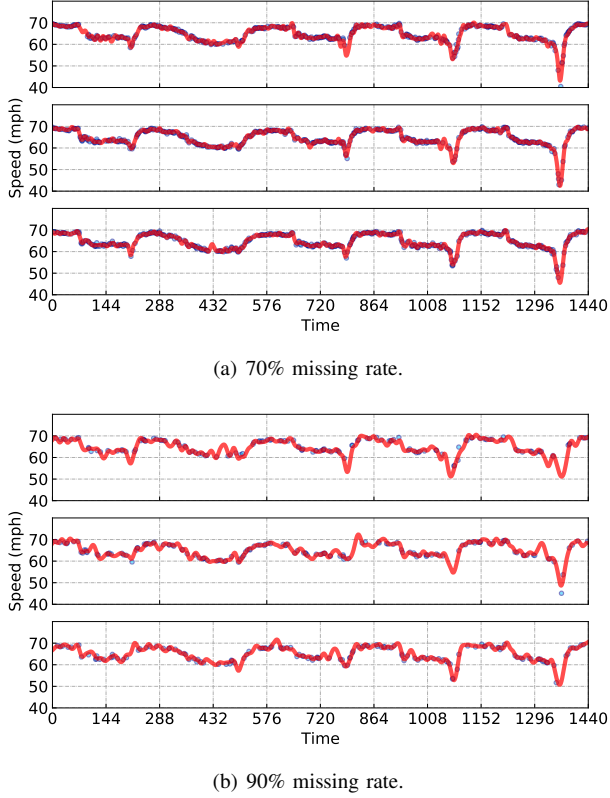


Fig. 6: Multivariate traffic time series imputation by LCR on the PeMS-4W dataset. We choose the traffic speed time series of the first three road segments during the first five days for illustration. Note that blue circles and red curves indicate the partial observations and the reconstructed time series, respectively.

the Laplacian kernel and set the kernel of the RGB channels as the first column of an identity matrix. Following the idea of LCR-2D (see the 2D separable kernel in Eq. (42)), the three-dimensional (3D) separable kernel based on Laplacian kernels is given by

$$\mathcal{K} \triangleq \ell_r \otimes_{\text{outer}} \ell_c \otimes_{\text{outer}} \ell_{RGB} \in \mathbb{R}^{M \times N \times 3}, \quad (52)$$

with

$$\begin{cases} \ell_r = (2\tau, \underbrace{-1, \dots, -1}_{\tau}, 0, \dots, 0, \underbrace{-1, \dots, -1}_{\tau})^\top \in \mathbb{R}^M, \\ \ell_c = (2\tau, \underbrace{-1, \dots, -1}_{\tau}, 0, \dots, 0, \underbrace{-1, \dots, -1}_{\tau})^\top \in \mathbb{R}^N, \\ \ell_{RGB} = (1, 0, 0)^\top \in \mathbb{R}^3, \end{cases} \quad (53)$$

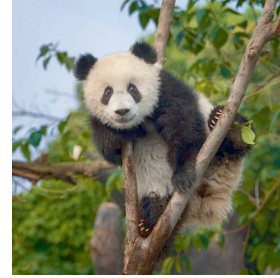
corresponding to the rows, the columns, and the RGB channels. The notation  $\otimes_{\text{outer}}$  denotes the outer product of vectors. The kernel size is  $\tau \in \mathbb{N}^+$ , which takes  $\tau \leq \frac{1}{2}(\min\{M, N\} - 1)$ .

As a result, the optimization problem of three-dimensional LCR (LCR-3D) can be formulated as follows,

$$\begin{aligned} \min_{\mathcal{X}} \quad & \|\mathcal{C}(\mathcal{X})\|_* + \frac{\gamma}{2} \|\mathcal{K} \star \mathcal{X}\|_F^2 \\ \text{s.t.} \quad & \|\mathcal{P}_\Omega(\mathcal{X} - \mathcal{Y})\|_F \leq \epsilon, \end{aligned} \quad (54)$$

where the definitions of circulant tensor and 3D circular convolution are naturally extended from LCR-2D as described in Eq. (43). In what follows, we utilize the same scheme of the ADMM framework on the aforementioned LCR models and adapt it to the LCR-3D algorithm. Notably, to assess the performance of image inpainting, we use the Peak Signal-to-Noise Ratio (PSNR, the larger the better) as the metric.

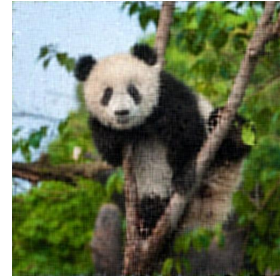
Fig. 7(a) shows a color image of size  $512 \times 512 \times 3$ . We randomly remove 90% pixels as missing pixels (i.e., 90% missing rate, see Fig. 7(b)), implying three missing values at all RGB channels in each masked pixel. In our LCR-3D model, we set the hyperparameters as  $\lambda = 1 \times 10^{-5}$ ,  $\eta = 10^2 \lambda$ , and  $\tau = 2$ . For comparison, we set the hyperparameter  $\gamma$  as  $\gamma = \lambda$  and  $\gamma = 10^{-10} \lambda \rightarrow 0$  (referring to LCR-3D without Laplacian regularization, i.e., CircNNM), respectively. Fig. 7(c) and 7(d) show the recovered images by the LCR-3D model. It demonstrates that LCR-3D can achieve more accurate inpainting results in the presence of Laplacian regularization over CircNNM.



(a) Original image.



(b) Incomplete image.



(c) Recovered image by the LCR-3D with  $\gamma = \lambda$ . Here, PSNR = 25.82dB.



(d) Recovered image by the LCR-3D with  $\gamma = 1 \times 10^{-10} \lambda$ . Here, PSNR = 23.38dB.

Fig. 7: Color image inpainting results of LCR-3D on the 90% randomly masked missing pixels.

Fig. 8(a) shows a more challenging image inpainting scenario, i.e., (row, column)-masked missing pixels in an image. This scenario also refers to the missing slice recovery [4]. We consider the LCR-3D model with different hyperparameter  $\gamma$ . Observing the inpainting results as shown in Fig. 8(b), 8(c), and 8(d), LCR-3D with  $\gamma = 10\lambda$  performs significantly better than CircNNM (i.e., refers to LCR-3D with  $\gamma = 10^{-10} \lambda \rightarrow 0$ ). Notably, as the conventional tensor completion models are not well-suited to such scenario, CircNNM with a circulant structure is capable of revealing global low-rankness property and reconstructing missing slices in an image tensor. In the

LCR-3D model, Laplacian kernels reinforce the low-rank completion with both global and local consistency.

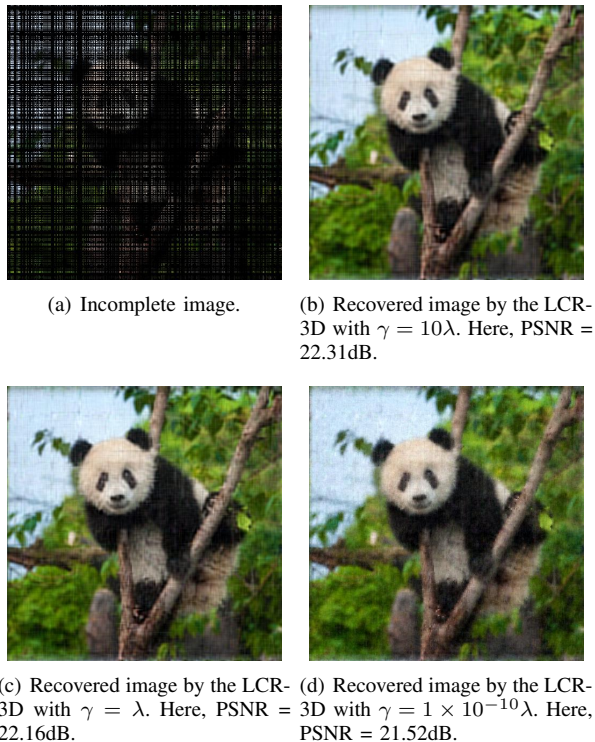


Fig. 8: Color image inpainting results of LCR-3D on the 50% row-masked and 50% column-masked missing pixels. The whole missing rate is about 75%.

### VIII. CONCLUSION

In this study, we focus on reconstructing spatiotemporal traffic data from partial observations. To model the local trends in traffic time series, we introduce a Laplacian kernel for temporal regularization in the form of circular convolution, which allows one to encode local correlations in time series. Following that definition, we propose an LCR model that integrates the temporal regularization into a circulant-matrix-based low-rank model for characterizing global and local trends in traffic time series. When developing the solution algorithm, we borrow the properties of circulant matrix and circular convolution, and prove that the proposed LCR model has a fast implementation through FFT. To be specific, the nuclear norm minimization with Laplacian temporal regularization can be converted into an  $\ell_1$ -norm minimization in complex space. Beyond univariate time series imputation, the modeling idea of LCR can be easily adapted to multivariate and even multidimensional time series imputation tasks.

In the numerical experiments, we conduct both univariate and multivariate time series imputation tasks on several real-world traffic datasets. For the fully observed data, LCR can produce denoised and smooth time series. For the sparse and noisy traffic data, LCR can accurately reconstruct traffic time series with the elimination of data noises, demonstrating the importance of Laplacian temporal regularization. On the

large-scale dataset, LCR outperforms the baseline models and demonstrates strong generalization to high-dimensional problems due to the efficient implementation and relatively low time complexity.

This study provides insight into spatiotemporal data modeling and shows the importance of jointly modeling global and local trends in time series data. We find an elegant formula that bridges the gap between low-rank models and graph Laplacian models; in the meanwhile, the formula leads to a fast implementation through FFT. Without loss of generality, the most basic modeling idea of the proposed LCR models can be easily extended from univariate time series imputation to multidimensional time series imputation, also showing to be extremely useful in the inverse problems such as image inpainting.

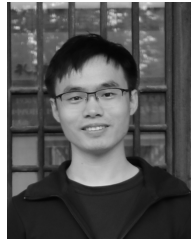
### ACKNOWLEDGMENT

Xinyu Chen would like to thank the Institute for Data Valorisation (IVADO) and the Interuniversity Research Centre on Enterprise Networks, Logistics and Transportation (CIRRELT) for providing the PhD Excellence Scholarship to support this study.

### REFERENCES

- [1] L. Li, X. Su, Y. Zhang, Y. Lin, and Z. Li, "Trend modeling for traffic time series analysis: An integrated study," *IEEE Transactions on Intelligent Transportation Systems*, vol. 16, no. 6, pp. 3430–3439, 2015.
- [2] E. J. Candes and Y. Plan, "Matrix completion with noise," *Proceedings of the IEEE*, vol. 98, no. 6, pp. 925–936, 2010.
- [3] J.-F. Cai, E. J. Candès, and Z. Shen, "A singular value thresholding algorithm for matrix completion," *SIAM Journal on optimization*, vol. 20, no. 4, pp. 1956–1982, 2010.
- [4] T. Yokota, B. Erem, S. Guler, S. K. Warfield, and H. Hontani, "Missing slice recovery for tensors using a low-rank model in embedded space," in *Proceedings of the IEEE conference on computer vision and pattern recognition*, 2018, pp. 8251–8259.
- [5] R. Yamamoto, H. Hontani, A. Imakura, and T. Yokota, "Fast algorithm for low-rank tensor completion in delay-embedded space," in *Proceedings of the IEEE/CVF Conference on Computer Vision and Pattern Recognition*, 2022, pp. 2058–2066.
- [6] G. Liu and W. Zhang, "Recovery of future data via convolution nuclear norm minimization," *IEEE Transactions on Information Theory*, 2022.
- [7] G. Liu, "Time series forecasting via learning convolutionally low-rank models," *IEEE Transactions on Information Theory*, vol. 68, no. 5, pp. 3362–3380, 2022.
- [8] D. Cai, X. He, J. Han, and T. S. Huang, "Graph regularized nonnegative matrix factorization for data representation," *IEEE transactions on pattern analysis and machine intelligence*, vol. 33, no. 8, pp. 1548–1560, 2010.
- [9] X. Mao, K. Qiu, T. Li, and Y. Gu, "Spatio-temporal signal recovery based on low rank and differential smoothness," *IEEE Transactions on Signal Processing*, vol. 66, no. 23, pp. 6281–6296, 2018.
- [10] L. Xiong, X. Chen, T.-K. Huang, J. Schneider, and J. G. Carbonell, "Temporal collaborative filtering with bayesian probabilistic tensor factorization," in *Proceedings of the 2010 SIAM international conference on data mining*. SIAM, 2010, pp. 211–222.
- [11] H.-F. Yu, N. Rao, and I. S. Dhillon, "Temporal regularized matrix factorization for high-dimensional time series prediction," *Advances in neural information processing systems*, vol. 29, 2016.
- [12] X. Chen, C. Zhang, X.-L. Zhao, N. Saunier, and L. Sun, "Nonstationary temporal matrix factorization for multivariate time series forecasting," *arXiv preprint arXiv:2203.10651*, 2022.
- [13] F. Sedighin, A. Cichocki, T. Yokota, and Q. Shi, "Matrix and tensor completion in multiway delay embedded space using tensor train, with application to signal reconstruction," *IEEE Signal Processing Letters*, vol. 27, pp. 810–814, 2020.

- [14] Z. Chen and A. Cichocki, "Nonnegative matrix factorization with temporal smoothness and/or spatial decorrelation constraints," *Laboratory for Advanced Brain Signal Processing, RIKEN, Tech. Rep.*, vol. 68, 2005.
- [15] Y. Wang, Y. Zhang, X. Piao, H. Liu, and K. Zhang, "Traffic data reconstruction via adaptive spatial-temporal correlations," *IEEE Transactions on Intelligent Transportation Systems*, vol. 20, no. 4, pp. 1531–1543, 2018.
- [16] X. Chen, Y. Chen, N. Saunier, and L. Sun, "Scalable low-rank tensor learning for spatiotemporal traffic data imputation," *Transportation research part C: emerging technologies*, vol. 129, p. 103226, 2021.
- [17] X. Chen, M. Lei, N. Saunier, and L. Sun, "Low-rank autoregressive tensor completion for spatiotemporal traffic data imputation," *IEEE Transactions on Intelligent Transportation Systems*, 2021.
- [18] X. Chen and L. Sun, "Bayesian temporal factorization for multidimensional time series prediction," *IEEE Transactions on Pattern Analysis and Machine Intelligence*, 2021.
- [19] J. Luttinen and A. Iljin, "Variational gaussian-process factor analysis for modeling spatio-temporal data," *Advances in neural information processing systems*, vol. 22, 2009.
- [20] T. Zhou, H. Shan, A. Banerjee, and G. Sapiro, "Kernelized probabilistic matrix factorization: Exploiting graphs and side information," in *Proceedings of the 2012 SIAM international Conference on Data mining*. SIAM, 2012, pp. 403–414.
- [21] M. Lei, A. Labbe, Y. Wu, and L. Sun, "Bayesian kernelized matrix factorization for spatiotemporal traffic data imputation and kriging," *IEEE Transactions on Intelligent Transportation Systems*, 2022.
- [22] A. J. Smola and R. Kondor, "Kernels and regularization on graphs," in *Learning theory and kernel machines*. Springer, 2003, pp. 144–158.
- [23] N. Rao, H.-F. Yu, P. K. Ravikumar, and I. S. Dhillon, "Collaborative filtering with graph information: Consistency and scalable methods," *Advances in neural information processing systems*, vol. 28, 2015.
- [24] P. C. Hansen, J. G. Nagy, and D. P. O'leary, *Deblurring images: matrices, spectra, and filtering*. SIAM, 2006.
- [25] J. Wright and Y. Ma, *High-dimensional data analysis with low-dimensional models: Principles, computation, and applications*. Cambridge University Press, 2022.
- [26] S. L. Brunton and J. N. Kutz, *Data-driven science and engineering: Machine learning, dynamical systems, and control*. Cambridge University Press, 2022.
- [27] E. Candes and B. Recht, "Exact matrix completion via convex optimization," *Communications of the ACM*, vol. 55, no. 6, pp. 111–119, 2012.
- [28] A. Sandryhaila and J. M. Moura, "Discrete signal processing on graphs: Graph fourier transform," in *2013 IEEE International Conference on Acoustics, Speech and Signal Processing*. IEEE, 2013, pp. 6167–6170.
- [29] H. Bristow, A. Eriksson, and S. Lucey, "Fast convolutional sparse coding," in *Proceedings of the IEEE Conference on Computer Vision and Pattern Recognition*, 2013, pp. 391–398.
- [30] B. Wohlberg, "Efficient convolutional sparse coding," in *2014 IEEE International Conference on Acoustics, Speech and Signal Processing (ICASSP)*. IEEE, 2014, pp. 7173–7177.
- [31] F. Heide, W. Heidrich, and G. Wetzstein, "Fast and flexible convolutional sparse coding," in *Proceedings of the IEEE Conference on Computer Vision and Pattern Recognition*, 2015, pp. 5135–5143.
- [32] J. Yang, W. Yin, Y. Zhang, and Y. Wang, "A fast algorithm for edge-preserving variational multichannel image restoration," *SIAM Journal on Imaging Sciences*, vol. 2, no. 2, pp. 569–592, 2009.
- [33] G. Liu, Z. Lin, S. Yan, J. Sun, Y. Yu, and Y. Ma, "Robust recovery of subspace structures by low-rank representation," *IEEE transactions on pattern analysis and machine intelligence*, vol. 35, no. 1, pp. 171–184, 2012.
- [34] E. O. Brigham, *The fast Fourier transform and its applications*. Prentice-Hall, Inc., 1988.
- [35] C. K. Williams and C. E. Rasmussen, *Gaussian processes for machine learning*. MIT press Cambridge, MA, 2006, vol. 2, no. 3.
- [36] C. Chen, K. Petty, A. Skabardonis, P. Varaiya, and Z. Jia, "Freeway performance measurement system: mining loop detector data," *Transportation Research Record*, vol. 1748, no. 1, pp. 96–102, 2001.



**Xinyu Chen** (Student Member, IEEE) received the B.S. degree in Traffic Engineering from Guangzhou University, Guangzhou, China, in 2016, and M.S. degree in Transportation Information Engineering & Control from Sun Yat-Sen University, Guangzhou, China, in 2019. He is currently a Ph.D. student with the Civil, Geological and Mining Engineering Department, Polytechnique Montreal, Montreal, QC, Canada. His current research centers on machine learning, spatiotemporal data modeling, and intelligent transportation systems.



**Zhanhong Cheng** received his Ph.D. degree from McGill University. He received his B.S. and M.S. degrees from Harbin Institute of Technology, Harbin, China. He is now a Postdoc researcher in the Department of Civil Engineering at McGill University, Montreal, QC, Canada. His research interests include public transportation, travel behavior modeling, spatiotemporal forecasting, and machine learning in transportation.



**Nicolas Saunier** received an engineering degree and a Doctorate (Ph.D.) in computer science from Telecom ParisTech, Paris, France, respectively in 2001 and 2005. He is currently a Full Professor with the Civil, Geological and Mining Engineering Department at Polytechnique Montreal, Montreal, QC, Canada. His research interests include intelligent transportation, road safety, and data science for transportation.



**Lijun Sun** (Senior Member, IEEE) received the B.S. degree in civil engineering from Tsinghua University, Beijing, China, in 2011, and the Ph.D. degree in civil engineering (transportation) from the National the University of Singapore in 2015. He is currently an Assistant Professor in the Department of Civil Engineering, McGill University, Montreal, QC, Canada. His research centers on intelligent transportation systems, machine learning, spatiotemporal modeling, travel behavior, and agent-based simulation.